Determination of the Three-Dimensional Structure of the Bifunctional α-Amylase/Trypsin Inhibitor from Ragi Seeds by NMR Spectroscopy[†,‡]

Stefan Strobl,[§,||] Peter Mühlhahn,[||] Reimond Bernstein,[||] Ronald Wiltscheck,[||] Klaus Maskos,[§] Martina Wunderlich,[§] Robert Huber,[||] Rudi Glockshuber,*[,§] and Tad A. Holak*[,||]

Max-Planck-Institut für Biochemie, D-82152 Martinsried, FRG, and Institut für Molekularbiologie und Biophysik, Eidgenössische Technische Hochschule−Hönggerberg, CH-8093 Zürich, Switzerland

Received February 6, 1995; Revised Manuscript Received April 24, 1995[⊗]

ABSTRACT: The three-dimensional structure of the bifunctional α-amylase/trypsin inhibitor (RBI) from seeds of ragi (*Eleusine coracana* Gaertneri) has been determined in solution using multidimensional ^1H and ^{15}N NMR spectroscopy. The inhibitor consists of 122 amino acids, with 5 disulfide bridges, and belongs to the plant α-amylase/trypsin inhibitor family for which no three-dimensional structures have yet been available. The structure of the inhibitor was determined on the basis of 1131 interresidue interproton distance constraints derived from nuclear Overhauser enhancement measurements and 52 ϕ angles, supplemented by 9 ψ and 51 χ_1 angles. RBI consists of a globular four-helix motif with a simple "up-and-down" topology. The helices are between residues 18−29, 37−51, 58−65, and 87−94. A fragment from Val 67 to Ser 69 and Gln 73 to Glu 75 forms an antiparallel β-sheet. The fold of RBI represents a new motif among the serine proteinase inhibitors. The trypsin binding loop of RBI adopts the "canonical", substrate-like conformation which is highly conserved among serine proteinase inhibitors. The binding loop is stabilized by the two adjacent α-helices 1 and 2. This motif is also novel and not found in known structures of serine proteinase inhibitors. The three-dimensional structure of RBI together with biochemical data suggests the location of the α-amylase binding site on the face of the molecule opposite to the site of the trypsin binding loop. The RBI fold should be general for all members of the RBI family because conserved residues among the members of the family form the core of the structure.

Serine protease inhibitors are widespread in the biosphere and are found in bacteria as well as in eukaryotic cells. On the basis of sequence identities, these proteins are divided into at least 13 distinct classes [for reviews, see Laskowski and Kato (1980), Laskowski (1986), Laskowski et al. (1987), and Richardson (1991)]. Representative three-dimensional structures have been determined for most of these families (Bode & Huber, 1992). Although their overall protein folds are different, their common feature is a structurally conserved binding loop, which protrudes into the active site of the corresponding serine protease in a substrate-like fashion.

The α-amylase/trypsin inhibitor family (also termed cereal inhibitor family) is a relatively new class of plant inhibitors found in cereal seeds (Richardson, 1991; Laskowski & Kato, 1980). It currently comprises 24 members with known sequences and an average size of about 120 amino acids (Figure 1). This class of proteins is characterized by a high content of cysteines that form four or five intramolecular disulfide bridges (Maeda et al., 1983a,b; Poerio et al., 1991). All functional members of the cereal inhibitor family are either inhibitors of mammalian α-amylases or trypsin. The bifunctional α-amylase/trypsin inhibitor from ragi (*Eleusine coracana* Gaertneri, Indian finger millet) (RBI)[1] is the only member possessing both functions simultaneously. The amino acid sequence of RBI has been determined and consists of 122 residues with 10 cysteines forming 5 intramolecular disulfide bonds (Campos & Richardson, 1983). RBI shares between 22% and 66% sequence identity with the other members of the family (Figure 1). Biochemical data suggested that its binding to trypsin and α-amylase is located in mutually exclusive binding sites since the inhibitor is capable of forming a ternary complex with trypsin and α-amylase (Shivaraj & Pattabiraman, 1981).

We have decided to determine the three-dimensional structure of RBI as it represents both types of inhibitory

[†] This work was supported by the Deutsche Forschungsgemeinschaft [Project H6, Sonderforschungbereich 207 of the Ludwig-Maximilians Universität (grant to T.A.H.) and Gl 159/1-1 and Gl 159/1-2 (grants to R.G.)] and the Fonds der Chemischen Industrie (grant to M.W.).

[‡] Coordinates of the final structures of RBI and the complete list of NMR constraints have been deposited in the Brookhaven Protein Data Bank under the file name 1BIP.

* To whom correspondence should be addressed.

[§] Institut für Molekularbiologie und Biophysik.

[||] Max-Planck-Institut für Biochemie.

[⊗] Abstract published in *Advance ACS Abstracts,* June 1, 1995.

[1] Abbreviations: RBI, bifunctional α-amylase/trypsin inhibitor from seeds of ragi (*Eleusine coracana* Gaertneri, Indian Finger Millet); P1, P2, P3 and P1′, P2′, P3′, inhibitor residues amino-terminal and carboxy-terminal of the scissile peptide bond, respectively; BPTI, bovine basic pancreatic trypsin inhibitor; CMTI, *Cucurbita maxima* trypsin inhibitor; LDTI, leech-derived tryptase inhibitor; SDS−PAGE, sodium dodecyl sulfate−polyacrylamide gel electrophoresis; Tris, tris(hydroxymethyl)-aminomethane; WAI 0.28, wheat α-amylase inhibitor 0.28; WAI 0.53, wheat α-amylase inhibitor 0.53; MOPS, 3-(*N*-morpholino)propanesulfonic acid; IPTG, isopropyl β-D-thiogalactoside; 2D, two dimensional; 3D, three dimensional; CD, circular dichroism; CT, constant time; D_2O, deuterated water; DQF-COSY, double-quantum-filtered homonuclear correlated spectroscopy; NMR, nuclear magnetic resonance; NOE, nuclear Overhauser effect; NOESY, two-dimensional NOE spectroscopy; HMQC, heteronuclear multiquantum coherence spectroscopy; HSQC, heteronuclear single-quantum coherence spectroscopy; HNHA, 3D $^1H^N-^{15}N^H-^1H^\alpha$ correlation spectrum; TOCSY (HOHAHA), total correlation spectroscopy (homonuclear Hartmann−Hahn spectroscopy); TPPI, time-proportional phase incrementation; RMSD, root mean square difference; rms, root mean square; SA, simulated annealing; ⟨SA⟩, an ensemble of the SA structures; (SA)m, the structure obtained by constrained minimization of the mean structure (the mean structure is obtained by averaging the coordinates of the ⟨SA⟩ structures).

0006-2960/95/0434-8281$09.00/0

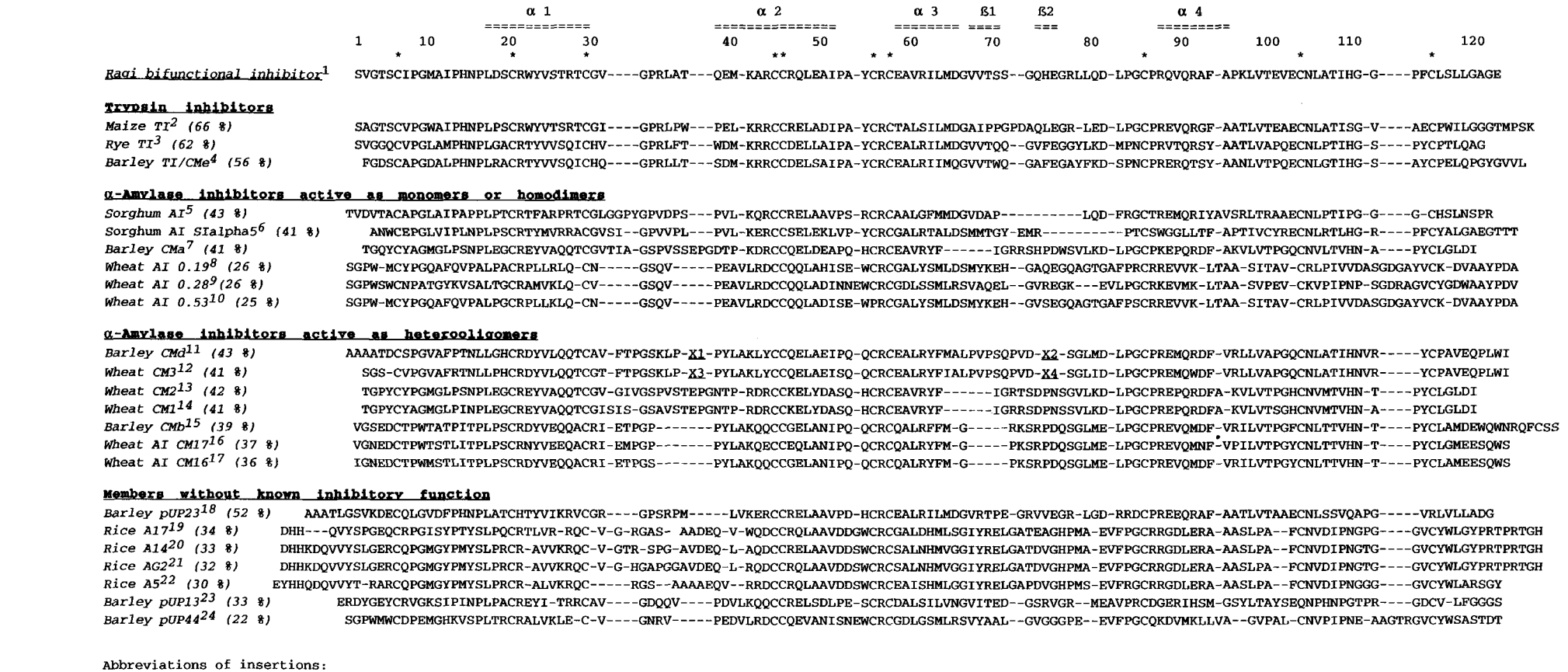

Abbreviations of insertions:
Barley CMd: X1 = EWMTSAELNYPGQ; X2 = PSTGNVGQ; *Wheat CM3*: X3 = EWMTSASIYSPGK; X4 = PRSGNVGE;

FIGURE 1: Alignment of the RBI sequence with known sequences of other members of the α-amylase/trypsin inhibitor family. The number of sequences shown is limited to proteins exhibiting significant sequence identity over the whole range of the RBI sequence. Signal sequences were omitted. The N-termini of the proteins were either determined by protein sequencing or represent the putative cleavage site for the signal peptidase. Footnotes: (1) Campos and Richardson (1983); (2) Mahoney et al. (1984); (3) Lyons et al. (1987); (4) Odani et al. (1983a); (5, 6) Bloch and Richardson (1992); (7) Garcia-Maroto et al. (1990); (8) Maeda et al. (1983a,b); (9) Kashlan and Richardson (1981); (10) Maeda et al. (1985); (11) Halford et al. (1988); (12, 14) Garcia-Maroto (1990); (13) Gautier et al. (1991); (15) Medina-Acazar et al. (1993); (16) Lullien et al. (1991); (17) Gautier et al. (1990); (18) Lazaro et al. (1988a); (19) Izumi et al. (1992); (20, 21, 22) Adachi et al. (1993); (23) Paz-Ares et al. (1986); (24) Lazaro et al. (1988b).

activities and as no structural information is presently available on any protein of this family. Recently, the crystallization and preliminary X-ray investigation of RBI were published (Srinivasan et al., 1991), but the three-dimensional structure of the protein has not been reported so far. In this paper we describe the determination of the secondary and three-dimensional structures of recombinant RBI, its disulfide bond pattern, and the sequential assignment of its NMR resonances. The secondary structure of RBI consists of both α-helical and β-structure elements. The secondary structure topology and the three-dimensional fold of the inhibitor are entirely different from known structures of the serine proteinase inhibitors. The structural features of RBI are discussed in terms of the conserved and substrate-like inhibition mode among serine proteinase inhibitors and in terms of possible sites of interaction with α-amylase. We also show that the overall structure of the inhibitor is not affected by cleavage at the reactive peptide bond responsible for trypsin binding.

MATERIALS AND METHODS

Materials. *N*-Acetylcysteine was purchased from Sigma, D_2O from Cambridge Isotope Laboratories, and [^{15}N]-ammonium chloride from Campro. Bacto-agar, Bacto-tryptone, and Bacto-yeast extract were purchased from Difco Laboratories (Detroit, MI). All other chemicals were from Merck (Darmstadt, Germany).

Purification of Recombinant RBI. The RBI samples used for our NMR studies were obtained by overproduction in *Escherichia coli* and subsequent three-step purification (Wunderlich & Glockshuber, 1993; K. Maskos, M. Wunderlich, and R. Glockshuber, unpublished results). For unlabeled samples, *E. coli* JM83 cells (Yanisch-Perron et al., 1985) carrying the plasmid pRBI-PDI (Wunderlich & Glockshuber, 1993) were grown in LB medium (Sambrook et al., 1989). The uniformly ^{15}N-labeled and [^{15}N]glycine/serine-labeled samples were produced in the *E. coli* strain BL21-(DE3) (Studier & Moffatt, 1986), carrying the plasmid pRBI-PDI-T7. This plasmid is a derivative of pRBI-PDI (Wunderlich & Glockshuber, 1993) and contains the T7 promoter instead of the lac promoter. The cells were grown on a M9 minimal medium (Sambrook et al., 1989) with [^{15}N]-ammonium chloride (1 g/L) as the only nitrogen source (uniformly ^{15}N-labeled) and on minimal medium supplemented with [^{15}N]glycine (1 g/L) and the residual unlabled amino acids, except for serine (selective [^{15}N]glycine/serine-labeling) (Griffey & Redfield, 1985). Bacteria were grown at 26 °C in the corresponding medium containing ampicillin (100 μg/mL). At an optical density at 550 nm of 1.0, IPTG and *N*-acetylcysteine were added to final concentrations of 1 and 5 mM, respectively. The bacteria were shaken for another 16 h, harvested by centrifugation, and suspended in 10 mM MOPS/NaOH, pH 7.0 (1/100 of the original volume). The cells were disrupted in a French pressure cell (1.374×10^8 Pa), and the lysate was centrifuged (48000*g*, 30 min, 4 °C). The soluble fraction was applied onto a DE-52 column (Whatman) and washed with 10 mM MOPS/NaOH, pH 7.0. The eluate was applied to an anhydrotrypsin affinity column (Cuatrecasas et al., 1968; Pusztai et al., 1988). The inhibitor was eluted by a shift to pH 2.3 with 150 mM NaCl and 5 mM HCl. These conditions lead to a dissociation of the anhydrotrypsin/RBI complex. The eluate contained pure RBI, but about 30% of the inhibitor was cleaved at Arg 34 due to residual trypsin activity and facilitated cleavage of RBI at acidic pH. To separate the native and cleaved forms of the inhibitor, the eluate was dialyzed against 20 mM Tris-HCl, pH 8.0, 100 mM NaCl, and 1 M ammonium sulfate and applied to a phenyl-Superose HR 5/5 column (Pharmacia, bed volume 2 mL). A linear gradient of ammonium sulfate (1.0−0.0 mM) was used to elute the proteins. The cleaved and native inhibitors were eluted at ammonium sulfate concentrations of 0.40 and 0.25 M, respectively. The purification was analyzed by SDS−PAGE (Fling & Gregerson, 1986) using 15% (v/v) acrylamide gels with subsequent silver staining. The yield of RBI was determined by its absorbance at 280 nm ($A_{280nm,1\ mg/mL,1\ cm} = 0.680$). The final yield of native RBI per liter bacterial culture was 0.41 mg for the unlabeled, 0.09 mg for the ^{15}N-labeled, and 0.10 mg for the [^{15}N]glycine/serine-labeled sample. Only the native inhibitor was used for NMR experiments. However, after extended time in the NMR tube, a significant amount (30−70%) of RBI was converted to the cleaved form, presumably due to minute amounts of trypsin released from the affinity column simultaneously with RBI.

Sample Preparation. The purified protein was dialyzed against 17 mM NaH_2PO_4 and 100 mM NaCl and then concentrated to 1.7−3.0 mM in a volume of 450 μL. After addition of 50 μL of D_2O (H_2O/D_2O = 9:1), the pH of the sample was 4.5. In some experiments, the pH of the sample was adjusted by addition of NaOH to 6.0. For recording spectra in D_2O, the samples were lyophilized and dissolved in D_2O. The pD was not corrected.

NMR Spectroscopy. All NMR experiments were carried out at 37 °C on a Bruker AMX600 spectrometer. The two-dimensional total correlation spectroscopy (TOCSY) was performed according to the method of Rance (1987) with the MLEV-17 sequence (Bax & Davis, 1985) for isotropic mixing and spin-lock periods of 40, 50, and 70 ms. The TOCSY pulse sequences included presaturation of the water resonance for measurements in H_2O (Gueron et al., 1991). Nuclear Overhauser enhancement spectroscopy (NOESY) experiments (Jeener et al., 1979; Ernst et al., 1987) were recorded with a pulse sequence in which the last 90° pulse was replaced by a jump−return sequence to suppress the water resonance (Plateau & Gueron, 1982). A homospoil pulse of 8 ms during the mixing time of 100 ms was also used. Essentially the same pulse sequences were used for the D_2O samples, with the exception that no water suppression was necessary. Usually 4096 complex data points were acquired in the time domain t_2 with a spectral width of 11.73 ppm in the F_2 dimension. A total of 800 increments in the time period t_1 with an F_1 spectral width of 11.73 ppm and 96 scans per t_1 value were added. Quadrature detection in the indirectly detected dimensions was obtained with the TPPI method (Marion & Wüthrich, 1983). A CT-COSY experiment (Girvin, 1994; Bax & Freeman, 1981) with an optimized constant time delay of 36 ms and 512 t_1 increments was recorded on the unlabeled H_2O sample. The other parameters were the same as in the 2D TOCSY and NOESY spectra. The 2D ^{1}H−^{15}N HMQC and HSQC correlation spectra were recorded as described by Summers et al. (1986) and Bodenhausen and Ruben (1980), respectively. The spectral parameters were the same as in the ^{15}N-separated 3D experiments [the number of increments in the ^{15}N time domain was larger (256)]. The 3D ^{1}H−^{15}N NOESY-HMQC (Zuiderweg & Fesik, 1989; Messerle et al., 1989) and ^{1}H−

^{15}N TOCSY-HMQC (Marion et al., 1989) spectra were recorded with a mixing time of 100 and 40 ms, respectively, and with 16 scans per t_1-t_2 pair. The spectral width and number of points acquired were 11.57 ppm and 90 complex points in ^1H (F_1), 44.11 ppm and 24 complex points in ^{15}N (F_2), and 5.24 ppm and 1024 real points in ^1H (F_3) with the ^1H (F_1), ^{15}N (F_2), and $^1H^N$ (F_3) carrier frequencies placed at 4.73, 109.82, and 7.83 ppm, respectively. All 3D spectra were processed with the software CC-NMR using linear prediction up to 256 data points along t_1 and 80 data points along t_2 to a final size of 256 × 80 × 1024 data points (Cieslar et al., 1993). After the peak-picking routine the assignment was carried out both manually and by use of program alfa (Bernstein et al., 1993a).

Finally, for the 3D ^{15}N-separated H^N-H^α correlation spectrum HNHA, which yielded the $^3J(H^N-H^\alpha)$ coupling constants from the ratio of the H^N-H^α cross peak to the H^N-H^N diagonal peak intensity (Vuister & Bax, 1993), the spectral width in the ^1H (F_2) dimension was 9.00 ppm and 128 complex points were acquired. The ^1H (F_2) carrier frequency was placed at 4.73 ppm, and 32 scans per t_1-t_2 pair were recorded. The spectrum was processed using linear prediction up to 64 data points along t_1 and 256 data points along t_2 to a final size of 64 × 256 × 1024 data points (Cieslar et al., 1993).

An amide exchange experiment, consisting of a series of 2D NOESY experiments, was carried out with RBI lyophilized from buffered H_2O and then freshly dissolved in D_2O. Within 24 h, three 2D data sets were recorded.

Stereospecific Assignments. For stereospecific assignment, $^3J_{a\beta}$ were extracted from the DQF-COSY in D_2O. Stereospecific assignments of $C^\beta H$ protons and methyl groups of valines and leucines were obtained using procedures described by Wagner et al. (1987) and Hyberts et al. (1987). $^3J_{H^\alpha N^H}$ coupling constants were measured mostly from the 3D ^{15}N-separated H^N-H^α correlation spectrum HNHA (see above) and a few from DQF-COSY spectra in H_2O. The apparent $^3J_{H^\alpha N^H}$ coupling constants measured from the splittings of the $NH-C^\alpha H$ cross peaks in DQF-COSY were corrected for line width using a method of Kim and Prestegard (1989).

Interproton Distance Constraints. NOEs were mainly derived from the 2D NOESY spectra in H_2O and D_2O at mixing times of 80 and 100 ms, respectively, and from the ^{15}N-filtered 2D NOESY spectra of [^{15}N]glycine/serine-labeled RBI. Some additional NOEs were obtained from the 3D ^{15}N-edited NOESY spectra. The intensities of the 2D NOE cross peaks were determined from volume integrals and converted into distance constraints according to the procedures described earlier (Holak et al., 1989). The distance bounds of the distance constraints were set to $d \pm 0.4$ Å for the distance constraints between 2.2 and 3.5 Å and to d −0.6 Å/+0.8 Å for distance constraints between 3.6 and 4.5 Å. All protons were explicitly defined in the dynamical simulated annealing calculations; in some cases, however, additional terms were added to the upper bounds that correspond to the pseudoatom correction introduced by Wüthrich (1986).

Torsion Angle Constraints. The distance constraints were supplemented with backbone ϕ torsion angle constraints derived from the $^3J_{H^\alpha H^N}$ coupling constant data (Table 1S, supporting information) and nine ψ angles (for the *trans*-peptide bond of the X-Pro residues; Wüthrich, 1986). The ϕ constraints were introduced in two stages. At the initial stage of the structure calculation, only those ϕ constraints were used which corresponded to the $^3J_{H^\alpha H^N}$ coupling constants larger than 8 Hz ($\phi = -120° \pm 40°$) (Pardi et al., 1984; Wüthrich, 1986). The rest of the ϕ constraints were introduced at a late stage of the refinement procedure (see below). Fifty-one χ_1 torsion angle constraints used in the calculations were derived from the stereospecifically assigned β-prochiral centers. The minimum ranges employed for the ϕ, ψ, and χ_1 torsion angles were ±20°, ±50°, and ±20°, respectively. A total of 223 non-NOE distance constraints were also present in the calculations (Holak et al., 1989).

Hydrogen Bond and Disulfide Bridge Constraints. RBI contains 10 cysteine residues; the S−S pairings were established during the determination of the secondary structure (see below). Since, however, Cys 44 and Cys 45, and Cys 55 and Cys 57, are close to each other, the initial structures were calculated without the presence of any disulfide bridges; i.e., neither corresponding disulfide distance constraints nor S−S bonds were introduced in the calculations (Holak et al., 1989; Wüthrich et al., 1986). These structures confirmed the predicted disulfide pairing, and in the final calculations the S−S bridges were treated as normal bonds.

Structure Calculations. Structure calculations were carried out essentially according to the basic protocol described previously (Holak et al., 1989). A total of 20 structures were calculated by a hybrid distance geometry−simulated annealing method (Holak et al., 1988, 1989) with the program X-PLOR 3.1 (Brünger, 1993). Minor modifications included simulation of 2D NOESY spectra in the final refinement stages to check whether NOE peaks calculated from NMR structures match experimental NOESY spectra (Bernstein et al., 1993b).

Structure Refinement. For the final refinement, the NOE tables were supplemented by 64 constraints for the 32 hydrogen bonds identified on the basis of the examination of the structures during the secondary structure analysis. Also, the NOE tables were supplemented at this stage with the ϕ constraints derived for the $J_{H^\alpha H^N}$ coupling constants equal to 8 Hz and ≤6 Hz (Holak et al., 1989). These ϕ constraints were introduced for residues for which ϕ's were close to the mean value (within ±20°) and fulfilled the Karplus relationship (Wüthrich, 1986) in structures calculated without the dihedral constraints.

RESULTS

Sequence-Specific Assignment of the ^1H and ^{15}N NMR Spectra. The NMR studies of RBI were carried out at both pH 4.5 and pH 6.0. The data at pH 4.5 are presented in this paper. The spectra measured at this pH were used for sequence-specific assignments. The data collected from the samples at higher pH served for confirmation of assignments. The 2D NOESY spectra at both pHs studied are very similar, indicating an identical structure of the protein within the pH range studied. An example of the $^1H-^{15}N$ HSQC spectrum of RBI is shown in Figure 2.

Trypsin can cleave RBI at its reactive peptide bond between residues Arg 34 and Leu 35 (Campos & Richardson, 1983). The RBI samples always contained mixtures of the cleaved and native inhibitor at various ratios, presumably due to minute amounts of trypsin released from the affinity column and copurified with RBI and to a facilitated cleavage

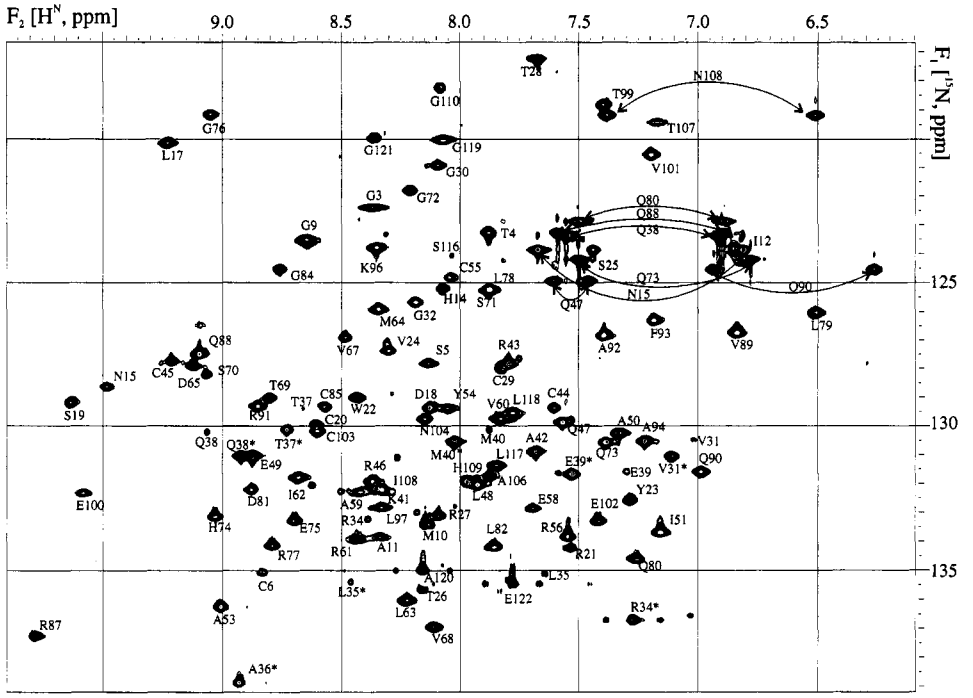

FIGURE 2: HSQC spectrum of uniformly labeled [^{15}N]RBI. Peaks of residues Trp 22 and Gly 30−Met 40 of the cleaved inhibitor are marked with an asterisk (see also the text). Cross peaks connected by arrows correspond to the side-chain NH_2 groups.

of RBI at acidic pH. The expression yield of the ^{15}N-labeled inhibitor was low (see Materials and Methods), and the protein also was obtained as a 1:2 mixture of native and cleaved forms. The use of the ^{15}N-labeled sample for assignments was therefore in part limited by these complications. Nevertheless, the ^{15}N-edited spectra provided helpful information for the sequential assignments (Figures 2 and 3). The NMR spectra of RBI were assigned with 2D and 3D NMR methods (Wüthrich, 1986) based on the following spectra: NOESY, TOCSY, and COSY, ^{1}H−^{15}N HSQC, ^{1}H−^{15}N TOCSY-HMQC, and ^{1}H−^{15}N NOESY-HMQC. Proton resonances of all backbone atoms were assigned with the exception of the amide and α-protons of residue 1 and the α-proton of proline 95 (see below). The complete spin systems of Pro 13, Pro 33, Pro 52, Pro 83, Pro 86, and Pro 112 could be identified. All of them are in the *trans* conformation because strong $H^{\delta}(i)^{Pro}$−$H^{\alpha}(i-1)$ NOE contacts were observed in the NOESY spectra. These contacts are diagnostic for the *trans* conformation of the proline amide bond (Wüthrich, 1986). Although it was not possible to assign the entire spin systems of the other three prolines (Pro 8, Pro 16, and Pro 95), there were enough data to conclude that they are also in a *trans* conformation. Both $H^N(i+1)$−$H^{\alpha}(i)^{Pro}$ and $H^{\delta}(i)^{Pro}$−$H^{\alpha}(i-1)$ connectivities could be observed for Pro 8 and Pro 16. In the case of Pro 95, neither the connectivity $H^{\delta}(i)^{Pro}$−$H^{\alpha}(i-1)$ nor a $H^{\alpha}(i)^{Pro}$−$H^{\alpha}(i-1)$ NOE (characteristic of the *cis* conformation) was observed. There were, however, two strong cross peaks at the Ala 94 amide proton frequency at 4.14 and 3.35 ppm in the NOESY spectrum. These resonances were tentatively assigned to the H^{δ} frequencies of Pro 95. We assumed that the $H^{\delta}(i)^{Pro}$−$H^{\alpha}(i-1)$ cross peaks were too weak to be observed and concluded from the presence of the $H^{\delta}(i)^{Pro}$−$H^N(i-1)$ cross peaks that Pro 95 is also in the *trans* conformation. A complete list of assignments is given in Table 1S of the supporting information.

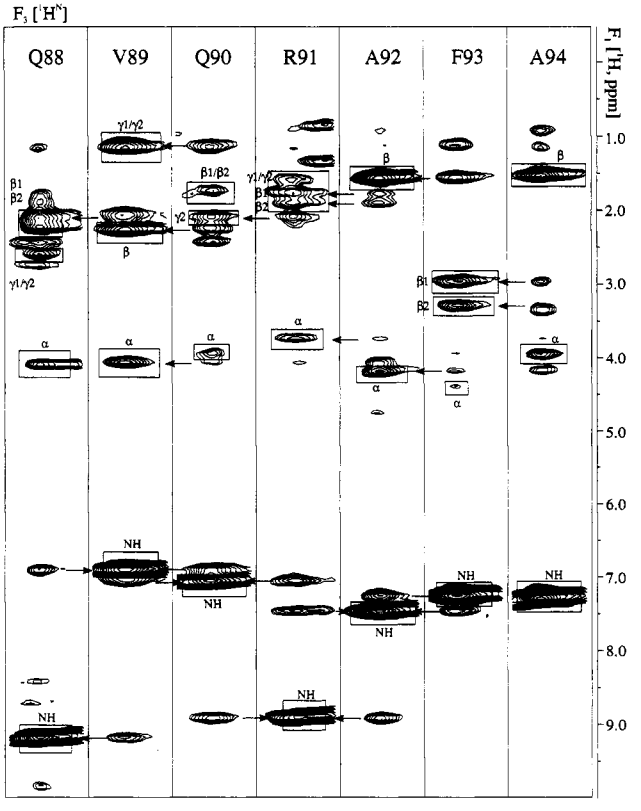

FIGURE 3: Strips from the 3D NOESY-HMQC spectrum of [^{15}N]-RBI showing resonances of residues Q88−A94 belonging to α-helix 4. The strips, ca. 65 Hz wide, are taken at the ^{15}N and $^1H^N$ chemical shifts of the residue of interest. Rectangles mark the intraresidual peaks; arrows indicate sequential connectivities.

Secondary Structure. Figure 4 summarizes the sequential and short-range NOEs observed in the spectra of RBI. These NOEs are the basis for the determination of the secondary structure of the protein (Wüthrich et al., 1984; Wüthrich, 1986). Many sequential $H^N(i)$−$H^N(i+1)$, $H^N(i)$−$H^N(i+2)$,

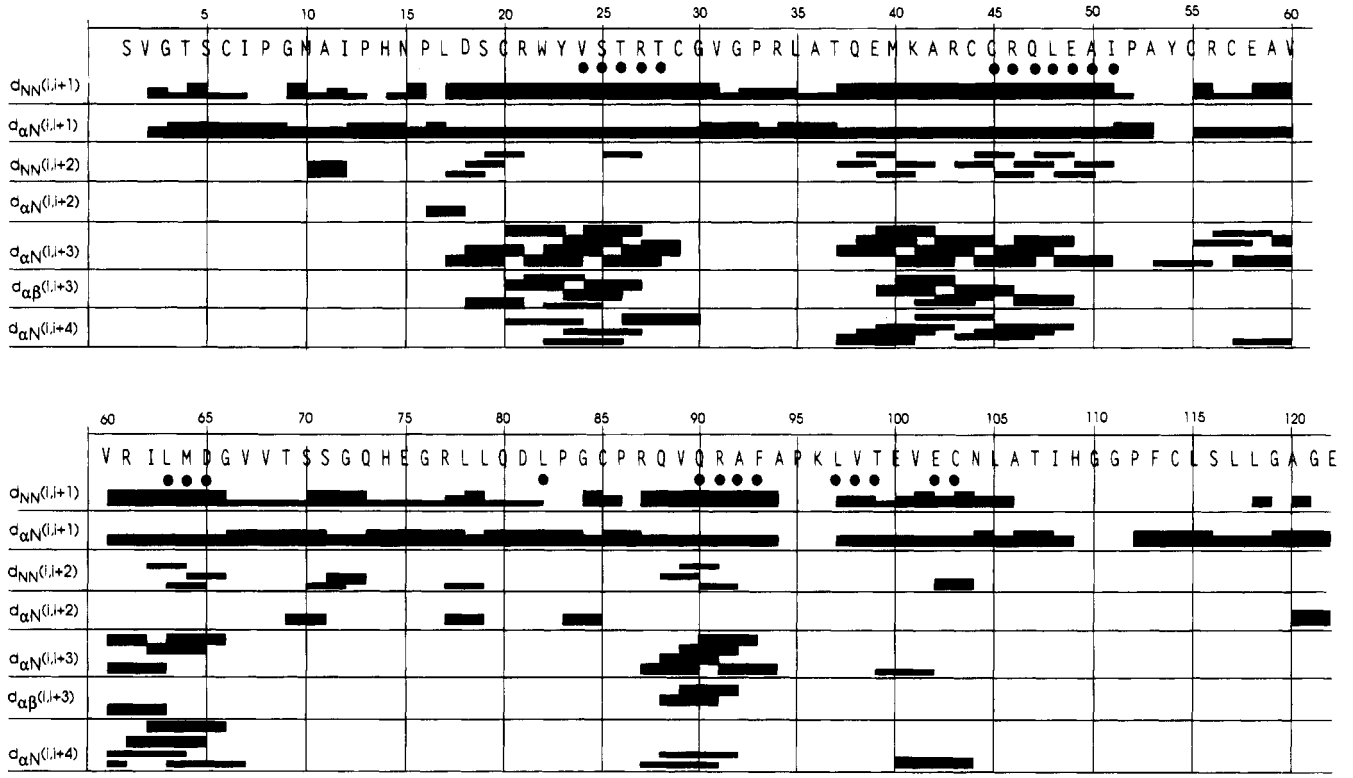

FIGURE 4: Summary of the short-range NOEs. The NOEs ($i - j < 5$), classified as weak, medium, and strong, are represented by the heights of the bars and were extracted from the NOESY spectra with mixing times of 100 ms. The $C^{\alpha}H(NH)(i)-C^{\delta}H(i+1)$ (Pro) NOE is shown along the same line as the $C^{\alpha}H(NH)(i)-NH(i+1)$ connectivities. Filled circles indicate NHs that did not exchange against D_2O after 6 h.

and $H^{\alpha}(i)-H^{N}(i+3)$ cross peaks, typical for α-helices, were found in the spectra (compare Figures 3 and 4). β-Strands were identified by the presence of strong sequential $H^{\alpha}(i)-H^{N}(i+1)$ cross peaks, weak intraresidual $H^{\alpha}(i)-H^{N}(i)$ cross peaks, and $H^{N}(i)-H^{N}(j)$ interstrand NOEs. As shown in Figure 5, four well-defined α-helices could be identified between residues 18−29, 37−51, 58−65, and 87−94. The two short β-strands, which form an antiparallel β-sheet, were found between residues 67−69 and 73−75. One interstrand $H^{\alpha}(i)-H^{\alpha}(j)$ cross peak and two interstrand $H^{N}(i)-H^{N}(j)$ cross peaks were observed, allowing the identification of three hydrogen bonds between the two different β-strands (Wüthrich, 1986). Another short β-strand may be present from residues 78 to 81. This region is characterized by strong sequential $H^{\alpha}(i)-{}^{N}H(i+1)$ and weak intraresidual $H^{\alpha}(i)-{}^{N}H(i)$ cross peaks. However, since these residues do not form any hydrogen bridges to another β-strand, and as some of the α-protons show an unusual high-field shift (L78 4.27 ppm, L79 4.33 ppm, D81 4.29 ppm; Table 1S, supporting information), this stretch of secondary structure could not be firmly described as β-strand. On the basis of its NOE cross-peak pattern, the turn between residues 82 and 85 could be ascribed to a type II turn.

Disulfide Bridge Pattern. Ten of the 122 residues of RBI are cysteines. All of them are involved in the formation of disulfide bridges (Campos & Richardson, 1983; Wunderlich & Glockshuber, 1993). Disulfide bridges between cysteine residues 6 and 55, 20 and 44, and 29 and 85 could unambiguously be identified on the basis of the diagnostic NOE connectivities $H^{\beta}(i)-H^{\beta}(j)$, $H^{\alpha}(i)-H^{\beta}(j)$, and $H^{\alpha}(i)-H^{\alpha}(j)$, where i and j are the residues in a S−S pair. To determine the location of the remaining two disulfide bridges, NOEs between one of the cysteines with another residue located in the vicinity of the second cysteine were used, for example, Cys 103 and Leu 48 (close to Cys 45); alternatively, long-range NOEs between residues which are in the vicinity of both cysteines were used, for example, Ala 53 and Pro 112, which are close to Cys 57 and Cys 114, respectively.

Cys 45 and Cys 57 are close to Cys 44 and Cys 55 in the primary sequence, respectively. In principle, therefore, alternate S−S bonding could be possible (Cys 57 to Cys 6, Cys 45 to Cys 20, and Cys 114 to Cys 55, for example). However, these configurations could be excluded, because at least one of the residues in all these putative pairs already had been assigned unequivocally to another disulfide bridge. The final disulfide bonding pattern of RBI is shown in Figure 6.

Comparison between the Native Inhibitor and the Inhibitor Cleaved by Trypsin at the Arg 34−Leu 35 Peptide Bond. As already mentioned, the RBI samples contained a mixture of native RBI and RBI cleaved by trypsin at the reactive Arg 34−Leu 35 peptide bond. As a consequence of the disruption of the primary sequence in the cleaved form, chemical shifts of the H^{N} and H^{α} protons of residues 30−40 and the chemical shifts of the aromatic protons of residue 22 were different from the corresponding shifts of the native form by more than 0.01 ppm (Table 2S, supporting information). There is no indication, however, that the secondary and tertiary structures of RBI are changed significantly between the two forms. Despite the substantially different chemical shifts of the native and cleaved inhibitor for residues 22 and 30−40, and some smaller differences in chemical shifts for other residues, the NOE intensities of the cross peaks were essentially identical for both forms, except for residues 32−38. Residues 32−38 appear to be unstructured in the cleaved form as no medium- and long-range NOEs could be detected in the spectra for these residues. Like

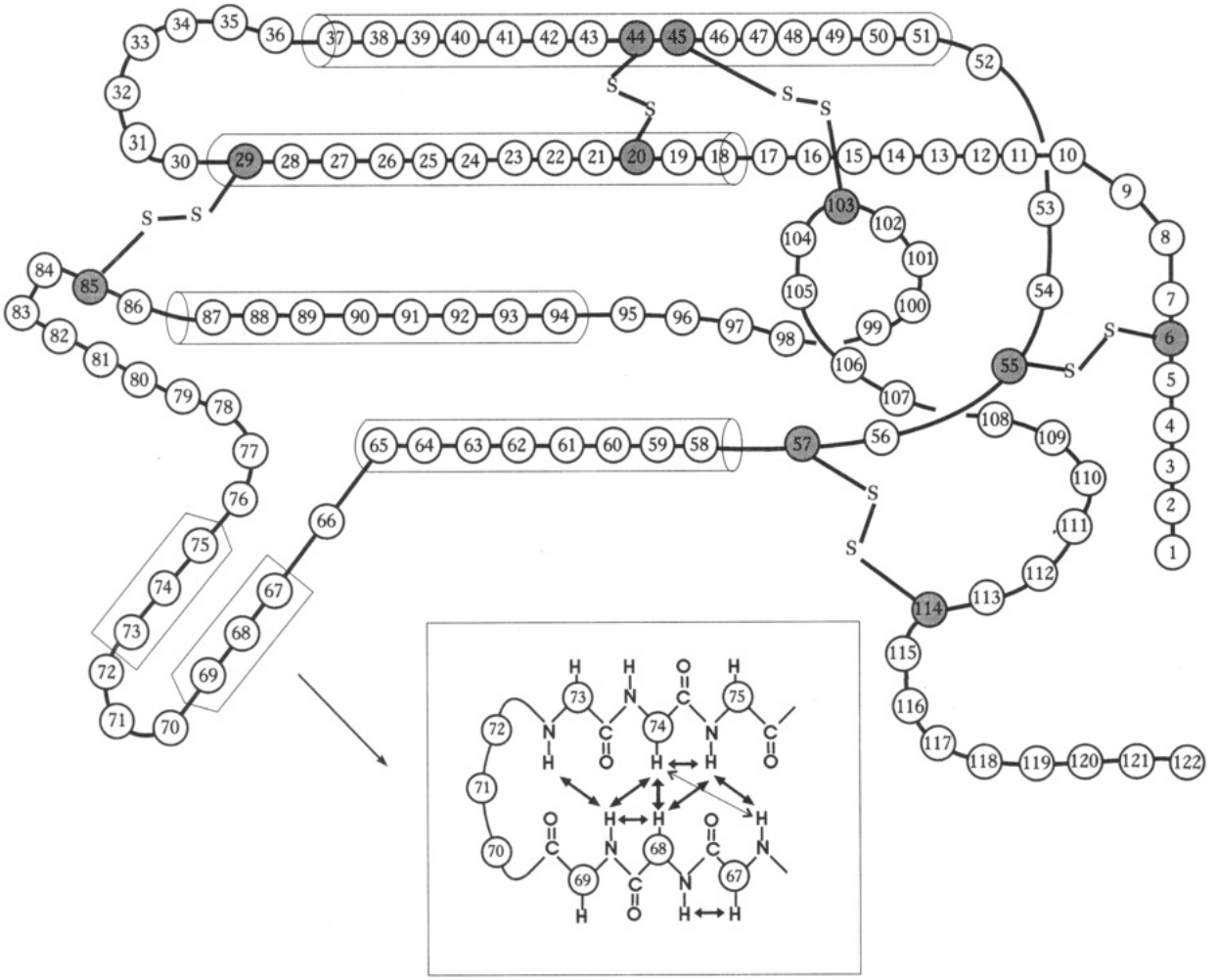

FIGURE 5: Schematic diagram of the secondary structure elements in RBI. Numbered circles represent the amino acids in the sequence; cysteines (dark circles) are emphasized. Cylinders indicate the position of α-helices; double-arrowed lines represent observed NOE connectivities, which mark the β-sheet.

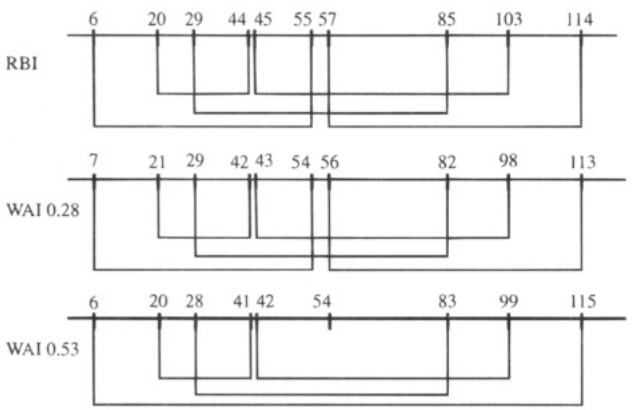

FIGURE 6: Schematic representation of the disulfide bond pattern of RBI and comparison with the known disulfide patterns of the related inhibitors WAI 0.28 and WAI 0.53.

native RBI, the cleaved inhibitor was fully stable during the NMR examination.

Tertiary Structure. The three-dimensional structure of RBI was calculated from 1131 approximate interresidue distance constraints. No intraresidue constraints were used. Also, some redundant ($i \rightarrow i+1$) constraints were not included in the list of NOEs. The $H^{\alpha}(i)-H^{N}(i+1)$ NOEs were always used for each pair of sequential residues. The other ($i \rightarrow i+1$) connectivities were included only when strong and unambiguous. Figure 7 shows a diagonal plot of the NOEs identified in the RBI NOESY spectra. The global folding of the polypeptide chain is uniquely defined due to the large number of NOEs in the core of the protein (Figures 8 and 9). An average number of interresidue constraints per residue in the core of the protein was 12. All structures satisfy the experimental constraints with small deviations from idealized covalent geometry (Table 1). The average atomic rms difference for heavy atoms in the core of RBI (residues 5−111) among the structures was 0.5 ± 0.2 Å for the backbone atoms and 1.3 ± 0.3 Å for all atoms. The average rms difference in the ϕ, ψ angles was <15° and <40°, respectively. Larger rms differences (ca. 3 Å for the backbone atoms and ca. 80° for the backbone torsion angles) were observed for the C- and N-terminus, for cysteine 55 (which makes the disulfide bridge with cysteine 5), and for Lys 96. For the two latter residues, the $J_{H^{N}H^{\alpha}}$ were ca. 6.5 Hz, preventing differentiation between positive and negative ϕ angles that were present in the calculated structures. This results in large RMSD for the ϕ angles whereas the RMSD for the atomic coordinates is small because the spatial positions of the C^{α} and nitrogen atoms are similar among the structures. Figure 10 indicates that the backbone of RBI is well determined with the exception of residues 1−5 and the C-terminal residues 111−122. These two regions of the protein seem to be completely unstructured. There were no long-range NOEs observed for these segments, and the

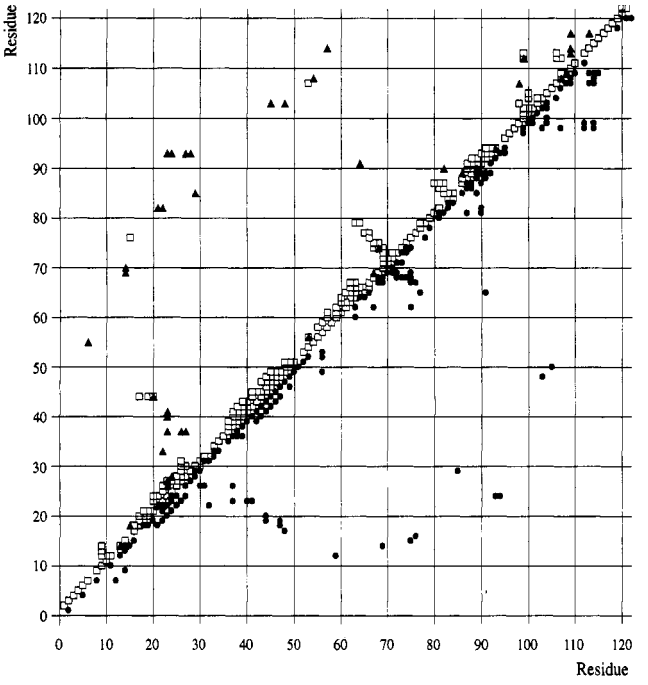

FIGURE 7: Diagonal plot of the interproton distance constraints used as input in the structure calculations. Backbone−backbone (squares) and side-chain−side-chain (triangles) interactions are plotted above the diagonal; backbone−side-chain (circles) constraints are shown below the diagonal.

sequential NOEs were much weaker than NOEs of the residues in the core of the protein. Also, the TOCSY peaks were stronger with noticeable reduction in the line widths compared to the peaks of residues in well-structured regions.

In general, conformations of the side chains are also well-defined. Panels A and C of Figure 10 show that only side chains of residues 1−6, 34, 43, 96, and 116−122 have greater rms differences in the calculated structures. This may be caused by the inability to make stereospecific assignments for these side-chain protons. A second reason is the lack of side-chain−side-chain contacts and long-range NOEs for these residues which makes it impossible to fix the side chains of these residues.

Most of the backbone torsion angles for non-glycine residues lie within the allowed regions of the Ramachandran plot (Figure 11). The few non-glycine residues that fall outside these regions are the residues that are located at the structural interfaces of helices and connecting loops.

The global fold of RBI and its secondary structure elements are shown in Figure 12A. The core of RBI consists of a globular four-helical motif with a simple "up-and-down" topology. The helices are between residues 18−29, 37−51, 87−94, and 58−65. A fragment from Val 67 to Thr 69 and Gln 73 to Glu 75 forms a antiparallel β-sheet with a reversal short loop at residues 70−72 (Figures 5, 9A, and 12A). The turn between residues 82 and 85 has a type II configuration. The RBI molecule has an approximate 2-fold symmetry with a symmetry plane perpendicular to the plane of Figure 9A and intersecting residues Leu 78 and Gly 110. Excepting the binding loop (see below), there are no similarities in the three-dimensional structure of RBI to other serine proteinase protein inhibitors for which structures have been solved up to now (Bode & Huber, 1992).

DISCUSSION

Secondary Structure. Up to now, secondary structure analysis of the cereal inhibitor family was based on circular dichroism spectra from a few inhibitors. The secondary structure content predicted from the CD spectra was for RBI approximately 10% α-helix and 30% β-strand (Alagiri & Singh, 1993), for the rye trypsin inhibitor and the rye α-amylase inhibitor, 36−37% α-helix and 18−20% β-strand, and 39−40% α-helix and 11−13% β-strand, respectively (Lyons et al., 1987), for the maize trypsin inhibitor, approximately 40% α-helix and 20% β-strand (Mahoney et al., 1984), and for the wheat α-amylase inhibitor 0.19, about 33% α-helix and 16% β-strand (Petrucci et al., 1976). Our data show unequivocally that the secondary structure of RBI contains 33% α-helices and about 7% β-structure elements. Four well-defined α-helices and at least two short β-strands, which form an antiparallel β-sheet, could be determined. This result is in disagreement with the prediction of Alagiri and Singh (1993) and in good agreement with the secondary structure predictions deduced from CD measurements for the other members of the inhibitor family. Within the pH range examined, the secondary structure elements are basically unaltered in the inhibitor cleaved at the reactive peptide bond Arg 34−Leu 35, indicating that the overall polypeptide fold is not significantly affected by the cleavage.

All ten cysteines in RBI are oxidized and form disulfide bridges, which obviously contribute to the overall stability of the protein against denaturation by heat or chemical denaturants (Shivaraj & Pattabiraman, 1981; Alagiri & Singh, 1993). The disulfide bridge pattern of two other members of the cereal inhibitor family, WAI 0.28 and WAI 0.53, had been determined before (Maeda et al., 1983a,b; Poerio et al., 1991). A comparison of disulfide bond patterns of RBI and WAI 0.28 reveals an identical disulfide topology (Figure 6), which together with its 26% amino acid similarity to RBI (Figure 1) suggests that the secondary structure elements are likely to be similar in WAI 0.28 and RBI. In contrast, the cystine pattern of WAI 0.53 differs from RBI and WAI 0.28 in that the 9 cysteine inhibitor lacks one disulfide and one of its disulfides (Cys 6/Cys 115) has a different connectivity pattern (Figure 6). However, the secondary structure elements are likely to be also conserved in WAI 0.53. Although Cys 6 and Cys 114 in RBI, corresponding to the Cys 6/Cys 115 disulfide in WAI 0.53, do not form a disulfide, the absence of Cys 55 would allow this alternative 6−114 cystine bridge. This assumption is supported both by the three-dimensional structure of RBI and by an engineered RBI mutant lacking Cys 55 (Maskos et al., unpublished results). Its CD spectrum and inhibitory activity against trypsin are comparable to those of the wild-type inhibitor. Moreover, like WAI 0.53, this RBI mutant forms a dimer due to oxidative dimerization via the free cysteine residue. Therefore, we propose that the secondary structure content is basically conserved throughout the whole cereal inhibitor family, independent of the different disulfide bridge patterns reported for some members of the protein family.

There are no similarities in the secondary structure topology of RBI to other members of the group of serine proteinase protein inhibitors for which three-dimensional structures have been solved up to now (Bode & Huber, 1992). The scaffold stabilizing the trypsin binding loop of RBI exhibits a new motif, quite different from the other

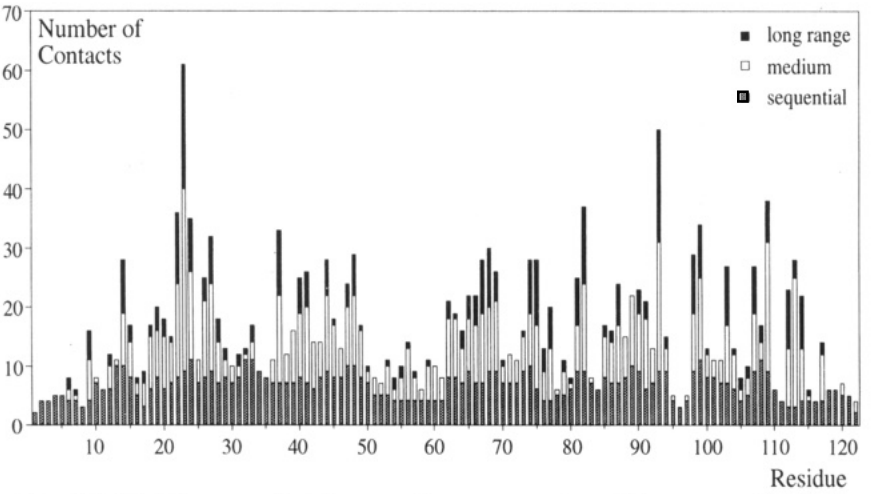

FIGURE 8: Plot of the number of NOE distance constraints per residue versus amino acid sequence of RBI. All constraints appear twice, once for each interacting residue. No intraresidue constraints were used.

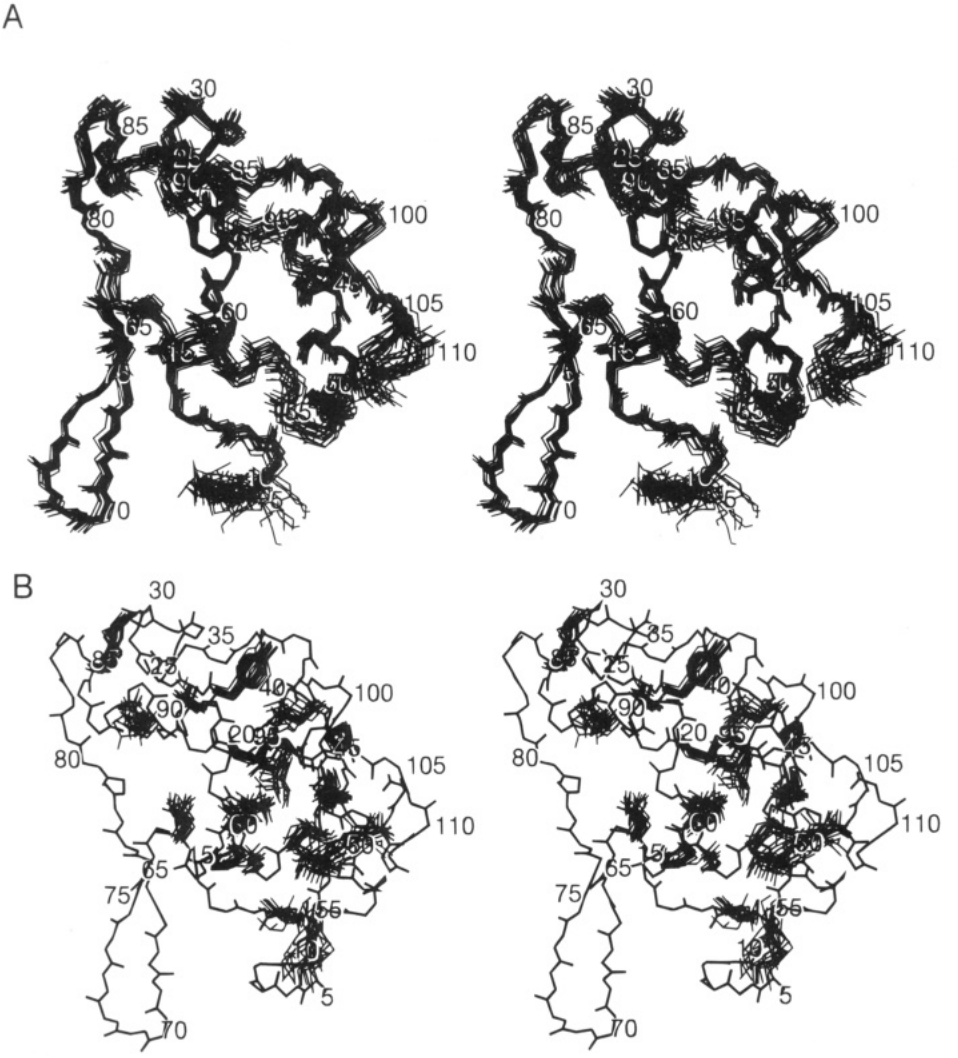

FIGURE 9: (A) Stereoview of the backbone atoms (N, C^{α}, C, and O) for residues 6−111 of RBI structures best fitted to N, C^{α}, and C atoms of the residues 13−114. (B) Stereo picture of the C^{α} tracing of one of the RBI structures with side chains of residues important for the protein core formation.

serine proteinase inhibitors, in that its binding loop is positioned between two α-helices.

The overall secondary structure content of 40% is rather low in RBI. However, this is not unexpected since a number of other small protein inhibitors of serine proteinases with high disulfide bond content such as Bowman−Birk-type inhibitors (Werner & Wemmer, 1991) and hirudins (Rydel et al., 1990; Folkers et al., 1989; Haruyama & Wüthrich, 1989) have also few secondary structure elements. Obviously, in these extraordinarily stable secretory proteins, intramolecular disulfide bond cross-linking compensates for a low content of stabilizing secondary structure.

Tertiary Structure. Conserved residues present in all members of the RBI family contribute to the apolar core of

Table 1: Average Deviations from Ideality, Energies of the Structures, and rms Differences between Experimental and Calculated Distance Constraints[a]

parameter	⟨SA⟩	(SA)m
deviations from idealized geometry		
bonds (Å) (1840)	0.004 ± 0.001	0.004
angles (deg) (3338)	0.815 ± 0.035	0.845
impropers (deg) (935)	0.538 ± 0.024	0.560
energies (kcal mol^{-1})		
E_{NOE}	237 ± 15	316
E_{tor}	0.180 ± 0.020	0.378
E_{repel}	203 ± 33	305
$E_{L\text{-}J}$	−354 ± 20	−230
no. of residual constraint violations (RMSD in Å) for all 1131 constraints		
0.2 ≤ RMSD ≤ 0.4	7 ± 4	20
0.4 < RMSD ≤ 0.5	1 ± 1	3
>0.5	0	0
rms differences from experimental constraints (Å)		
all (1131)	0.063 ± 0.009	0.094
sequential (458)	0.048 ± 0.008	0.044
interresidue ($\|i-j\| < 5$) (202)	0.054 ± 0.003	0.083
long ($\|i-j\| \geq 5$) (248)	0.072 ± 0.010	0.102
non-NOE distances (223)	0.003 ± 0.002	0.030
intraresidue (0)		

[a] ⟨SA⟩ represents an ensemble of the 20 final structures, (SA)m is the structure obtained by constrained minimization of the mean structure. The mean structure was obtained by averaging the coordinates of the 20 final ⟨SA⟩ structures best fitted to N, C^{α}, and C atoms of all residues except residues 1−6 and 110−122. The number of bond, angle, and improper terms is given in parentheses. Force constants used to calculate energy terms are the same as reported previously (Holak et al., 1989, Table 1). The rms deviations (in angstroms) from the interproton distance constraints were calculated as described in Holak et al. (1989). The number of distance constraints is given in parentheses. The hydrogen bond constraints are included in the long-range distance constraints.

the molecule (Figure 9B). None of these residues could directly form a contact with trypsin or α-amylase. Rather, residues conserved in the RBI family appear to be responsible for packing of the apolar core that defines the three-dimensional fold. The RBI fold should therefore be general for all members of the RBI family. Ten cysteines are almost completely conserved among all members of the family and appear to be primarily responsible for the stabilization of the overall fold. The only exceptions from the ten cysteine rule are the wheat inhibitor WAI 0.53[10] (lacking the fifth cysteine), barley pUp13[18] (lacking the tenth cysteine), and barley pUP13[23] (lacking the ninth cysteine) (Figure 1). WAI 0.53 differs from RBI in that one of its disulfides (Cys 6/Cys 115) has a different connectivity pattern and one disulfide is lacking. Nevertheless, the RBI fold seems to be conserved for this inhibitor too, and most probably it is also conserved for the barley pUp13[18] and pUP13[23]. Other residues from the core of the protein are also highly conserved throughout the family. These are hydrophobic residues, Pro 16, Leu 17, Val 24, Leu 48, Ile 51, Ala 59, Val 60, Leu 63, Leu 97, and Val 98, and two charged/polar residues, Arg 56 and Gln 90, which are completely buried (Figure 9B). Almost all these residues, together with Ile 12, are located at the interface between helix 1−2 and helix 3. Residues Val 24 and Leu 97, and additionally Tyr 23 and Val 102, underpin the course of the polypeptide that defines packing between the end of helix 1, the middle of helix 4, and residues of the C-terminal loops.

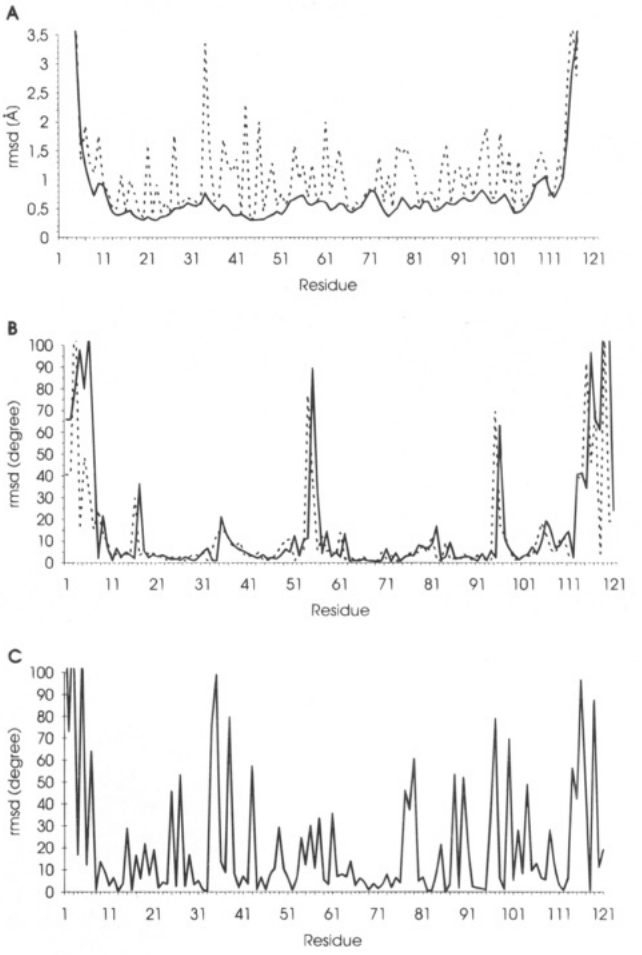

FIGURE 10: (A) Residue-based root mean square deviations of the atomic coordinates among the SA structures for the backbone atoms (N, C^{α}, C, and O, solid line) and non-hydrogen side-chain atoms (dashed line). (B) Residue-based rms deviations of the backbone ϕ (solid line) and ψ (dashed line) torsion angles for the 20 SA structures. (C) Residue-based rms deviations of the side-chain χ_1 torsion angles.

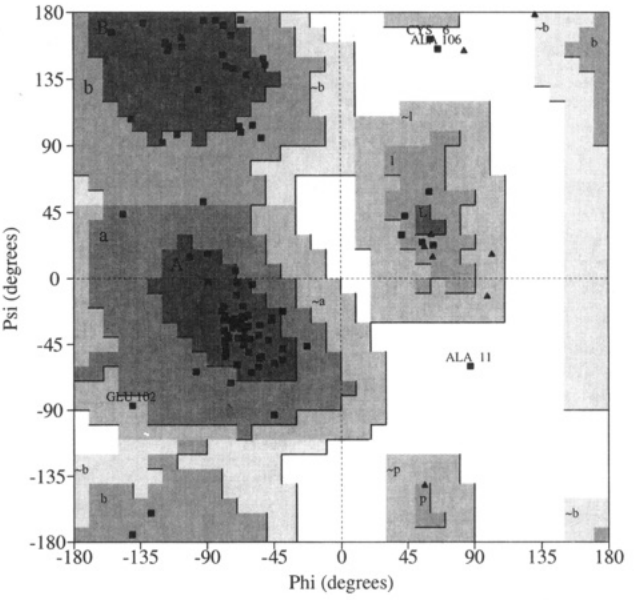

FIGURE 11: Ramachandran plot for the (SA)m structure of RBI. Glycine residues are represented by triangles.

Conformation of the Trypsin Binding Loop. The trypsin binding loop of RBI is connected to the core of the protein via helix 18−29, the disulfide bridge 29−85, α-helix 37−

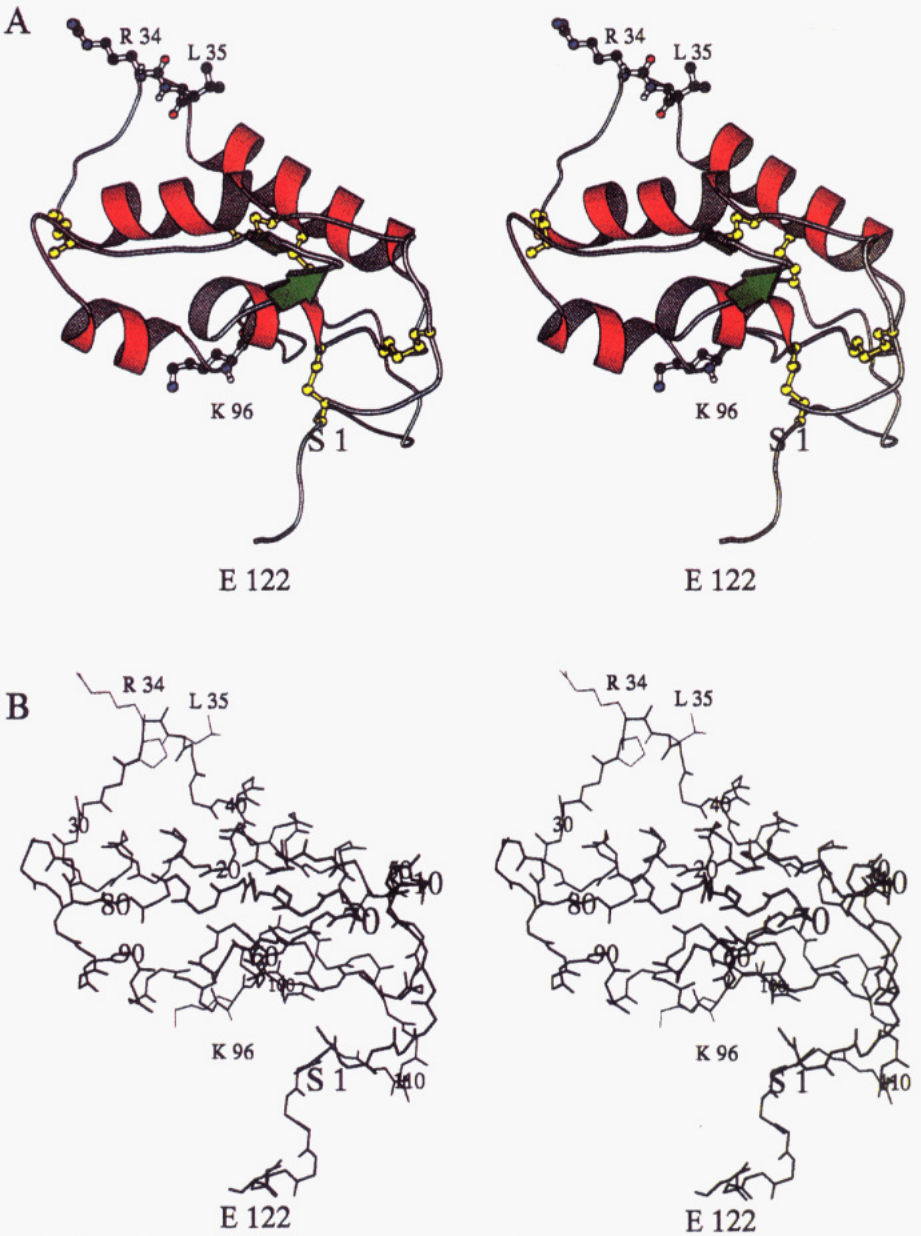

FIGURE 12: (A) Ribbon drawing of RBI showing the secondary structure, disulfide bridges, and side chains of residues R34, L35, and K96. (B) The (SA)m structure with details of the canonical conformation of the binding loop (residues 32−37). All backbone atoms, with the exception of hydrogen, are shown.

51, and disulfide bridges 44−20 and 45−103 (Figure 12). The conformation of the binding loop corresponds to the so-called "canonical" conformation observed for many other serine proteinase inhibitors, where the conformation of the residues surrounding the scissile bond (residues P3 to P3′) enables tight binding of the inhibitor to the target protease in a substrate-like manner (Bode & Huber, 1992). Within the canonical loop segment, the chain is in an extended conformation, such that the side chains surrounding the scissile bond (with the exception of P3) are exposed to the solvent or target protease and project away from the supporting scaffold. The typical features of the binding loop from P3 to P3′ comprise a main-chain conformation (i) of an antiparallel β-strand ($-140° < \phi < -120°$; $140° < \psi < 170°$) at the P3 position (except BPTI), (ii) of polyproline II ($-100° < \phi < -60°$; $139° < \psi < 180°$) at P2 and P1′, (iii) of an approximate 3_{10}-helix ($-120° < \phi < -95°$; $9° < \psi < 50°$) at P1, and (iv) of parallel β-strands ($-140° < \phi < -99°$; $70° < \psi < 120°$) at P2′ and P3′ (Bode & Huber, 1992). In RBI, all residues Gly 32 (P3), Pro 33 (P2), Arg 34 (P1), Leu 35 (P1′), Ala 36 (P2′), and Thr 37 (P3′) are in accord with these criteria: Arg 34, at position P1, is the primary determinant of specificity of the inhibitor, consistent with trypsin inhibition, and is exposed and poised for insertion into the specificity pocket. A proline residue is present at position P2 in RBI; proline at this position is also found in CMTI (Holak et al., 1989), LDTI-C (Mühlhahn et al., 1994), and ovomucoid inhibitors (Bode & Huber, 1992) and in all cases adopts the canonical conformation. For the ensemble of conformations of the binding loop in RBI the ϕ and ψ angles were Gly 32 120° ± 3° and 180° ± 4°, Pro 33 −65° ± 1° and 143° ± 3°, Arg 34 (P1) −114° ± 2° and 45° ± 5°, Leu 35 (P1′) −75° ± 1° and 173° ± 3°, and Ala 36 (P2′) −92° ± 1° and 62° ± 2°, respectively. The trypsin binding loop of RBI exhibits a new motif of connection to the protein core different from all other inhibitors in that its binding loop is stabilized and positioned between two α-helices (helices 1 and 2).

The α-Amylase Binding Site. In contrast to the well-established mechanisms of inhibition of serine proteinases by protein inhibitors (Laskowsky & Kato, 1980; Laskowsky, 1986; Bode & Huber, 1992) and the fact that their sites of interaction with the corresponding proteinases have been identified, relatively little is known about the mechanism by which protein inhibitors of α-amylases interact with their target enzymes. The only structural information available so far is the three-dimensional crystal structure of the complex between porcine α-amylase and tendamistat, an extraordinarily strong inhibitor of the enzyme. Tendamistat interacts with α-amylase near the polysaccharide binding site and thus appears to inhibit enzyme in a competitive manner (Wiegand et al., 1995).

Recent experiments on the inhibition of porcine α-amylases by RBI indicated a mixed-competitive inhibition mechanism (Maskos et al., unpublished results). Consequently, the RBI binding site of α-amylase must be different from the polysaccharide binding pocket, and a ternary complex between RBI, α-amylase, and polysaccharide substrate must exist.

Attempts to correlate sequence segments of the cereal inhibitors (Figure 1) with their inhibitory functions, in particular, the presence or absence of α-amylase inhibition, did not suggest which residues are essential for α-amylase binding. The existence, however, of a ternary complex between trypsin, RBI, and α-amylase excludes residues within or near the trypsin binding loop as candidates for the interaction with α-amylase (Shivaraj & Pattabirman, 1981; Maskos et al., unpublished results). Chemical modification experiments indicated that Lys 96 in RBI may be involved in binding to mammalian α-amylases (Shivaraj & Pattabirman, 1981; Alagiri & Singh, 1993). This is in accord with the three-dimensional structure of RBI, as the α-carbon of Lys 96 is located 23 Å away from the α-carbon of Arg 34 in the trypsin binding loop (Figure 12). The proposal that the inhibitor's Trp 22 and Tyr 23 residues are involved in α-amylase binding (Alagiri & Singh, 1993) is not supported by the RBI structure, as these residues are mainly involved in the stabilization of the trypsin binding loop.

ACKNOWLEDGMENT

We thank Wolfram Bode, Rick Engh, and Milton Stubbs for stimulating discussions and Rainer Deutzmann for determining the N-termini of native and cleaved RBI.

SUPPORTING INFORMATION AVAILABLE

Two tables of the ^{1}H and ^{15}N assignments for the native RBI and the inhibitor cleaved by trypsin at the Arg 34−Leu 35 peptide bond and a list of $J_{H^{\alpha}H^{N}}$ coupling constants (7 pages). Ordering information is given on any current masthead page.

REFERENCES

Adachi, T., Izumi, H., Yamada, T., Tanaka, K., Takeuchi, S., Nakamura, R., & Matsuda, T. (1993) *Plant Mol. Biol. 21*, 239−248.

Alagiri, S., & Singh, T. P. (1993) *Biochim. Biophys. Acta 1203*, 77−84.

Bax, A., & Freeman, R. (1981) *J. Magn. Reson. 44*, 542−561.

Bax, A., & Davis, D. G. (1985) *J. Magn. Reson. 65*, 355−366.

Bernstein, R., Cieslar, C., Ross, A., Oschkinat, H., Freund, J., & Holak, T. A. (1993a) *J. Biomol. NMR 3*, 245−251.

Bernstein, R., Ross, A., Cieslar, C., & Holak, T. A. (1993b) *J. Magn. Reson. B 101*, 185−188.

Bloch, C., Jr., & Richardson, M. (1992) *Protein Sequences Data Anal. 5*, 27−30.

Bode, W., & Huber, R. (1992) *Eur. J. Biochem. 204*, 433−451.

Bodenhausen, G., & Ruben, D. J. (1980) *Chem. Phys. Lett. 69*, 185−189.

Brünger, A. T. (1993) *X-PLOR Version 3.1 Manual*, Yale University, New Haven, CT.

Campos, F. A. P., & Richardson, M. (1983) *FEBS Lett. 152*, 300−304.

Cieslar, C., Ross, A., Zink, T., & Holak, T. A. (1993) *J. Magn. Reson. B 101*, 97−101.

Cuatrecasas, P., Wilchek, M., & Anfinsen, C. B. (1968) *Proc. Natl. Acad. Sci. U.S.A. 61*, 636.

Ernst, R. R., Bodenhausen, G., & Wokaun, A. (1987) *Principles of NMR in One and Two Dimension*, Clarendon Press, Oxford.

Fling, S. P., & Gregerson, D. S. (1986) *Anal. Biochem. 155*, 83−88.

Folkers, P. J. M., Clore, G. M., Driscoll, P. C., Dodt, J., Köhler, S., & Gronenborn, A. M. (1989) *Biochemistry 28*, 2601−2617.

Garcia-Maroto, F., Marana, C., Mena, M., Garcia-Olmedo, F., & Carbonero, P. (1990) *Plant Mol. Biol. 14*, 845−853.

Gautier, M. F., Alary, R., & Joudrier, P. (1990) *Plant Mol. Biol. 14*, 313−322.

Gautier, M. F., Alary, R., Lullien, V., & Joudrier, P. (1991) *Plant Mol. Biol. 16*, 333−334.

Girvin, M. E. (1994) *J. Magn. Reson. A 108*, 99−102.

Griffey, R. H., & Redfield, A. G. (1985) *Biochemistry 24*, 817−822.

Gueron, M., Plateau, P., & Decorps, M. (1991) *Progress Nucl. Magn. Reson. Spectrosc. 23*, 135−209.

Halford, N. G., Morris, N. A., Urwin, P., Williamson, M. S., Kasarda, D. D., Lew, E. J.-L., Kreis, M., & Shewry, P. R. (1988) *Biochim. Biophys. Acta 950*, 435−440.

Haruyama, H., & Wüthrich, K. (1989) *Biochemistry 28*, 4301−4312.

Holak, T. A., Kearsley, S. K., Kim, Y., & Prestegard, J. H. (1988) *Biochemistry 27*, 6135−6142.

Holak, T. A., Gondol, D., Otlewski, J., & Wilusz, T. (1989) *J. Mol. Biol. 210*, 635−648.

Hyberts, S. G., Mäki, W., & Wagner, G. (1987) *Eur. J. Biochem. 164*, 625−635.

Izumi, H., Adachi, T., Fujii, N., Matsuda, T., Nakamura, R., & Tanaka, K. (1992) *FEBS Lett. 302*, 213−216.

Jeener, J., Meier, B. H., Bachman, P., & Ernst, R. R. (1979) *J. Chem. Phys. 71*, 4546−4553.

Kashlan, N., & Richardson, M. (1981) *Phytochemistry 20*, 1781−1784.

Kim, Y., & Prestegard, J. H. (1989) *J. Magn. Reson. 84*, 9−13.

Laskowski, M., Jr. (1986) in *Toxicological Significance of Enzyme Inhibitors in Foods* (Freedman, M., Ed.) pp 1−17, Plenum Publishing Corp., New York.

Laskowski, M., Jr., & Kato, I. (1980) *Annu. Rev. Biochem. 49*, 593−626.

Laskowski, M., Jr., Kato, I., Kohr, W. J., Park, S. J., Tashiro, M., & Whatley, H. E. (1987) *Cold Spring Harbor Symp. Quant. Biol. 52*, 545−553.

Lazaro, A., Rodriguez-Palenzuela, P., Marana, C., Carbonero, P., & Garcia-Olmedo, F. (1988a) *FEBS Lett. 239*, 147−150.

Lazaro, A., Sanchez-Monge, R., Salcedo, G., Paz-Ares, J., Carbonero, P., & Garcia-Olmedo, F. (1988b) *Eur. J. Biochem. 172*, 129−134.

Lullien, V., Alary, R., Guirao, A., Joudrier, P., & Gautier, M. F. (1991) *Plant Mol. Biol. 17*, 1081−1082.

Lyons, A., Richardson, M., Tatham, A. S., & Shewry, P. R. (1987) *Biochim. Biophys. Acta 915*, 305−313.

Maeda, K., Hase, T., & Matsubara, H. (1983a) *Biochim. Biophys. Acta 743*, 52−57.

Maeda, K., Wakabayashi, S., & Matsubara, H. (1983b) *J. Biochem. 94*, 865−870.

Maeda, K., Wakabayashi, S., & Matsubara, H. (1985) *Biochim. Biophys. Acta 828*, 213−221.

Mahoney, W. C., Hermodson, M. A., Jones, B., Powers, D. D., Corfman, R. S., & Reek, J. R. (1984) *J. Biol. Chem. 259*, 8412−8416.

Marion, D., & Wüthrich, K. (1983) *Biochem. Biophys. Res. Commun. 113*, 967−974.
Marion, D., Driscoll, P. C., Kay, L. E., Wingfield, P. T., Bax, A., Gronenborn, A., & Clore, G. M. (1989) *Biochemistry 28*, 6150−6156.
Medina-Alcazar, J., Hueros, G., & Carbonero, P. (1993) *Plant Mol. Biol. 23*, 535−542.
Messerle, B. A., Wider, G., Otting, G., Weber, C., & Wüthrich, K. (1989) *J. Magn. Reson. 85*, 608−613.
Mühlhahn, P., Czisch, M., Morenweiser, R., Habermann, B., Engh, R. A., Sommerhoff, C. P., Auerswald, E. A., & Holak, T. A. (1994) *FEBS Lett. 355*, 290−296.
Odani, S., Koide, T., & Ono, T. (1983) *J. Biol. Chem. 258*, 7998−8003.
Pardi, A., Billeter, M., & Wüthrich, K. (1984) *J. Mol. Biol. 180*, 741−751.
Paz-Ares, J., Ponz, F., Rodriguez-Palenzuela, P., Lazaro, A., Hernandez-Lucas, C., Garcia-Olmedo, F., & Carbonero, P. (1986) *Theor. Appl. Genet. 71*, 842−846.
Petrucci, T., Rab, A., Tomasi, M., & Silano, V. (1976) *Biochim. Biophys. Acta 420*, 288−297.
Plateau, P., & Gueron, M. (1982) *J. Am. Chem. Soc. 104*, 7310−7311.
Poerio, E., Caporale, C., Carrano, L., Pucci, P., & Buonocore, V. (1991) *Eur. J. Biochem. 199*, 595−600.
Pusztai, A., Grant, G., Steward, J. C., & Watt, W. B. (1988) *Anal. Biochem. 172*, 108−112.
Rance, M. (1987) *J. Magn. Reson. 74*, 557−564.
Richardson, M. (1991) *Methods Plant Biochem. 5*, 259−305.
Rydel, T. J., Ravichandran K. G., Tulinsky, A., Bode, W., Huber, R., Roitsch, C., & Fenton, J. W., II (1990) *Science 249*, 277−280.
Sambrook, J., Fritsch, E. F., & Maniatis, T. (1989) *Molecular Cloning: A Laboratory Manual*, 2nd ed., Cold Spring Harbor Laboratory Press, Cold Spring Harbor, NY.
Shivaraj, B., & Pattabiraman, T. N. (1981) *Biochem. J. 193*, 29−36.
Srinivasan, A., Raman, A., & Singh, T. P. (1991) *J. Mol. Biol. 222*, 1−2.
Studier, F. W., & Moffatt, B. A. (1986) *J. Mol. Biol. 189*, 113−130.
Summers, M. F., Marzilli, L. G., & Bax, A. (1986) *J. Am. Chem. Soc. 108*, 4285−4294.
Vuister, G. W., & Bax, A. (1993) *J. Am. Chem. Soc. 115*, 7772−7777.
Wagner, G., Braun, W., Havel, T. F., Schaumann, T., Go, N., & Wüthrich, K. (1987) *J. Mol. Biol. 196*, 611−639.
Werner, M. H., & Wemmer, D. E. (1991) *Biochemistry 30*, 3356−3364.
Wiegand, G., Epp, O., & Huber, R. (1995) *J. Mol. Biol. 247*, 99−100.
Wunderlich, M., & Glockshuber, R. (1993) *J. Biol. Chem. 268*, 24547−24550.
Wüthrich, K. (1986) *NMR of Proteins and Nucleic Acids*, Wiley, New York.
Wüthrich, K., Billeter, M., & Braun, W. (1984) *J. Mol. Biol. 180*, 715−740.
Yanisch-Perron, C., Vieira, J., & Messing, J. (1985) *Gene 33*, 103−119.
Zuiderweg, E. R. P., & Fesik, S. W. (1989) *Biochemistry 28*, 2387−2391.

BI950264B